Inorganic Chemistry

ARTICLE

pubs.acs.org/IC

Selective Hydrolysis of Phosphate Monoester by a Supramolecular Phosphatase Formed by the Self-Assembly of a Bis(Zn^{2+}-cyclen) Complex, Cyanuric Acid, and Copper in an Aqueous Solution (Cyclen = 1,4,7,10-Tetraazacyclododecane)

Mohd Zulkefeli,[†,‡] Asami Suzuki,[†] Motoo Shiro,[§] Yosuke Hisamatsu,[†] Eiichi Kimura,[⊥] and Shin Aoki*[,†,¶]

[†]Faculty of Pharmaceutical Sciences and [¶]Center for Technologies against Cancer, Tokyo University of Science, 2641 Yamazaki, Noda, Chiba 278-8510, Japan

[‡]Faculty of Pharmacy, Universiti Teknologi MARA, Puncak Alam, Selangor 42300, Malaysia

[§]X-ray Research Laboratory, Rigaku Corporation, 3-9-12 Matsubaracho, Akishima, Tokyo 196-8666, Japan

[⊥]Faculty of Science, Shizuoka University, 836 Ohya, Suruga-ku, Shizuoka 422-8529, Japan

Supporting Information

ABSTRACT: In Nature, organized nanoscale structures such as proteins and enzymes are formed in aqueous media via intermolecular interactions between multicomponents. Supramolecular and self-assembling strategies provide versatile methods for the construction of artificial chemical architectures for controlling reaction rates and the specificities of chemical reactions, but most are designed in hydrophobic environments. The preparation of artificial catalysts that have potential in aqueous media mimicking natural enzymes such as hydrolases remains a great challenge in the fields of supramolecular chemistry. Herein, we describe that a dimeric Zn^{2+} complex having a 2,2′-bipyridyl linker, cyanuric acid, and a Cu^{2+} ion automatically assembles in an aqueous solution to form a 4:4:4 complex, which is stabilized by metal−ligand coordination bonds, $\pi-\pi$-stacking interactions, and hydrogen bonding and contains μ-$Cu_2(OH)_2$ cores analogous to the catalytic centers of phosphatase, a dinuclear metalloenzyme. The 4:4:4 complex selectively accelerates the hydrolysis of a phosphate monoester, mono(4-nitrophenyl)phosphate, at neutral pH.

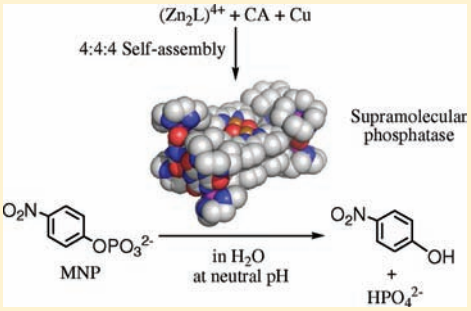

INTRODUCTION

Phosphorylation and dephosphorylation of proteins and enzymes are important processes in intracellular regulation. Dephosphorylation of phosphoserine and phosphothreonine residues in proteins is catalyzed by protein phosphatases, which catalyze the reverse reaction of protein kinases.[1] The structures of several metallophosphatases have been reported, including alkaline phosphatase (AP) from *Escherichia coli* containing $Zn^{2+}-Zn^{2+}$ centers and kidney bean purple acid phosphatase (KBPAP) and Ser/Thr protein phosphatase I, which contain $Zn^{2+}-Fe^{3+}$ centers.[2] Although the metal cations in these phosphatases are different and the amino acid sequences of the enzymes are not related, the structures of their active sites are similar in that they include dimetallic diamond cores containing two metal cations, which are coordinated by amino acids and hydroxide ions.[2]

Although chemical models for phosphatases have been developed,[3,4] artificial compounds that catalyze the hydrolysis of phosphonic acid monoester, such as mono(4-nitrophenyl) phosphate (MNP), are limited, and most contain two metal−macrocyclic polyamine complexes connected by covalent bonds.[5] Moreover, none functions as a catalyst for the hydrolysis of phosphate monoester.

Supramolecular strategies have been proven to afford powerful methodologies for the construction of structures for molecular recognition, molecular sensing, molecular storage, electronic devices, and reaction catalysts and drug delivery systems.[6,7] However, supramolecular systems that function as reaction pockets or catalysts in aqueous solutions remain limited,[8] and no example of a phosphatase mimic constructed by the self-assembly of molecular modules has been reported.

The coordination of organic anions to Zn^{2+}−macrocyclic polyamine complexes provides unique modules for the molecular recognition[9] and sensing[10] of biorelevant molecules, catalysts for asymmetric synthesis,[11] and three-dimensional molecular assembly.[12,13] We report herein on the preparation of a supramolecular complex formed via the reversible self-assembly of bis(Zn^{2+}-cyclen) containing a 2,2′-bipyridyl (bpy) linker **1** (cyclen = 1,4,7,10-tetraazacyclododecane),[10c] cyanuric acid (CA), and Cu^{2+} in an aqueous solution, as a result of metal−ligand coordination, $\pi-\pi$ stacking, and hydrogen-bond formation (Scheme 1). A dianion of CA (CA^{2-}) and **1** assemble in a 2:2 ratio to give **2**,

Received: May 20, 2011
Published: September 21, 2011

Scheme 1. Programmed Self-Assembling Formation of 4:4:4 Supermolecule 3 via 2:2 Supermolecule 2 and the Hydrolysis of MNP[a]

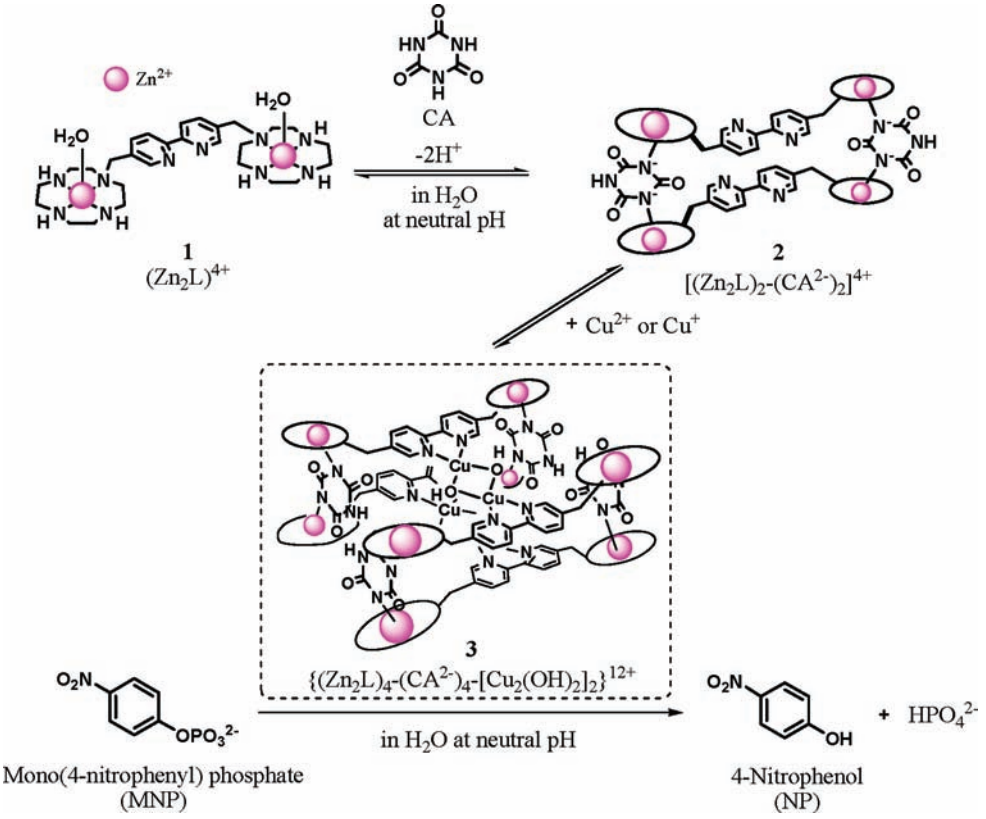

[a] The μ-$Cu_2(OH)_2$ center at the bottom side of **3** is omitted for clarity.

and the addition of Cu^{2+} or Cu^{+} to **2** induces the 2:4 complexation of **2** and Cu^{2+} to afford **3**, which is a 4:4:4 complex of **1**, CA^{2-}, and Cu^{2+}. Interestingly, **3** contains two μ-$Cu_2(OH)_2$ centers, which resemble the active centers of dinuclear metalloenzymes such as AP,[2] although contained metal ions are different. We describe the selective hydrolysis of MNP by **3** and the one-pot hydrolysis of bis(4-nitrophenyl) phosphate (BNP) to inorganic phosphate (HPO_4^{2-}) by combination with a natural enzyme, phosphodiesterase (PDE), under physiological conditions.

EXPERIMENTAL SECTION

General Information. All reagents and solvents were of the highest commercial quality and were used without further purification, unless otherwise noted. All aqueous solutions were prepared using deionized and distilled water. Bis(Co^{3+}-cyclen)anthracene complex **4** was synthesized according to the literature [$Co(NO_3)_2 \cdot 6H_2O$ was used for complexation].[5d] Good's buffers (Dojindo, pK_a at 20 °C) were obtained commercially: 2-[4-(2-hydroxyethyl)-1-piperazinyl]ethanesulfonic acid (HEPES), pK_a = 7.6; 3-(cyclohexylamino)propanesulfonic acid (CAPS), pK_a = 10.4; 2-(cyclohexylamino)ethanesulfonic acid (CHES), pK_a = 9.5; 3-[4-(2-hydroxyethyl)-1-piperazinyl]propanesulfonic acid (EPPS), pK_a = 8.0; 2-morpholinoethanesulfonic acid (MES), pK_a = 6.2. Stock aqueous solutions of 10 mM mono(4-nitrophenyl) phosphate (MNP), 10 mM bis(4-nitrophenyl) phosphate (BNP), and 10 mM 4-nitrophenol (NP) were prepared using deionized and distilled water and stored at 0 °C prior to use. A stock solution of 10 mM tris(4-nitrophenyl) phosphate (TNP) was prepared in ethanol (EtOH) and stored at 0 °C prior to use. Stock solutions of 10 mM 4-nitrophenyl acetate (NA) and 10 mM L-leucine-4-nitroanilide (Leu-NA) were prepared in MeCN and stored at 0 °C prior to use. Alkaline phosphatase (AP) from *E. coli* (EC.3.1.3.1) (suspension in 2.5 M $(NH_4)_2SO_4$) and phosphodiesterase I (PDE) from *Crotalus atrox* (EC 3.1.4.1) (crude dried venom) were purchased from Sigma Life Science. High-performance liquid chromatography (HPLC) experiments were carried out using a system consisting of two PU-980 intelligent HPLC pumps (JASCO, Japan), a UV-970 intelligent UV/vis detector (JASCO), a Rheodine injector (model 7125), and a Chromatopak C-R6A (Shimadzu, Japan). UV spectra were recorded on a JASCO V-550 spectrophotometer, equipped with a temperature controller unit at 25 ± 0.1 and 37 ± 0.1 °C. IR spectra were recorded on a JASCO FTIR-710 spectrophotometer at room temperature. Melting points were measured by a Yanaco MP-J3 Micro Melting Point apparatus without any correction. ^1H (300 MHz) and ^{13}C (75 MHz) NMR spectra at 25 ± 0.1 °C were recorded on a JEOL Always 300 spectrometer. 3-(Trimethylsilyl)-propionic-*2,2,3,3-d*$_4$ acid sodium salt in D_2O was used as the external reference for ^1H and ^{13}C NMR measurements. The p*D* values in D_2O were corrected for a deuterium isotope effect using p*D* = [pH-meter reading] + 0.40. Elemental analyses were performed on a Perkin-Elmer CHN 2400 series II CHNS/O analyzer at the Research Institute for Science and Technology, Tokyo University of Science. Thin-layer chromatography (TLC) and silica gel column chromatography were performed using a Merck Art. 5554 (silica gel) TLC plate and Fuji Silysia Chemical FL-100D, respectively.

Isolation of $2 \cdot 4NO_3^- \cdot 15H_2O$. $1 \cdot 4NO_3^- \cdot 5H_2O \cdot EtOH$[10c] (100 mg, 0.1 mmol), CA (12.6 mg, 0.1 mmol), and $NaNO_3$ (123 mg, 1.45 mmol) were dissolved in H_2O (3 mL) at room temperature, and the pH was adjusted to 7.5 ± 0.1 by the addition of aqueous NaOH. The whole

dx.doi.org/10.1021/ic201072q |*Inorg. Chem.* 2011, 50, 10113–10123

mixture was filtered and evaporated slowly for 1 week until colorless needlelike crystals of $2\cdot 4NO_3\cdot 15H_2O$ appeared (87 mg, 87% yield). Mp: >250 °C. IR (KBr): ν 3264, 2934, 1641, 1570, 1322, 1093, 948 cm^{-1}. ^1H NMR (300 MHz, D_2O/external TSP): δ 2.88 (40H, m, NCH_2), 3.06 (16H, m, NCH_2), 3.30 (8H, m, NCH_2), 4.06 (8H, br s, $ArCH_2$), 7.76−7.70 (8H, m, ArH), 8.25 (4H, m, ArH). ^{13}C NMR (75 MHz, D_2O/external TSP): δ 42.06, 43.75, 44.45, 48.48, 51.71, 121.93, 149.87, 160.45, 165.73. ESI-MS. Calcd for $C_{62}H_{98}N_{27}O_9Zn_4$ ($\{[Zn_2L]_2[CA]_2(NO_3)\}^{3+}$) ($M^{3+}$) $[Zn_2L]_2[CA]_2(NO_3)$: m/z 540.1730. Found: m/z 540.1731. Anal. Calcd for $C_{62}H_{128}N_{30}O_{33}Zn_4$: C, 35.74; H, 6.19, N, 20.17. Found: C, 35.21; H, 5.60; N, 20.45.

Isolation of $3\cdot 8NO_3^-\cdot 4I^-\cdot 31H_2O$. $2\cdot 4NO_3^-\cdot 15H_2O$ (30 mg, 0.014 mmol), CuI (6 mg, 0.03 mmol), and $NaNO_3$ (49 mg, 0.56 mmol) were dissolved in H_2O (3 mL), and the pH was adjusted to 7.5 ± 0.1 by the addition of aqueous NaOH. The whole mixture was filtered and concentrated slowly in vacuo for 1 week, and pale-blue crystals of $3\cdot 8NO_3^-\cdot 4I^-\cdot 31H_2O$ (26 mg, 75% yield) were obtained. Mp: >250 °C. IR (KBr): ν 3263, 2933, 1645, 1570, 1321, 1091, 947 cm^{-1}. Anal. Calcd for $C_{124}H_{260}N_{60}O_{71}Cu_4Zn_8I_4$: C, 29.71; H, 5.23; N,16.77. Found: C, 29.57; H, 4.89; N, 16.98.

Crystallographic Studies of $2\cdot 4NO_3^-\cdot 15H_2O$ and $3\cdot 8NO_3^-\cdot 4I^-\cdot 31H_2O$. Intensity data were collected on a Rigaku RAXIS-RAPID imaging-plate diffractometer with graphite-monochromated Cu Kα radiation. An empirical absorption correction was applied. The structures were solved by direct methods[14] and refined by full-matrix least-squares techniques. All calculations were performed using the Crystal Structure [version 3.80, Rigaku & RAC (2007)] except for refinements, which were performed with *SHELXL97*.[15]

Crystallographic Study of $2\cdot 4NO_3^-\cdot 15H_2O$. A colorless needle-shaped crystal (0.25 × 0.08 × 0.02 mm) in a twinning form was obtained after slow evaporation of an aqueous solution of **1** mixed with CA over a period of 1 week. The structure refinement was performed using reflection data of 1.1 Å resolution. Of the 15 waters, suggested by elemental analysis, only 7 were located: the residual ones were supposed to be contained in the voids of 312 $Å^3$ in the crystal and heavily disordered. Crystal data: $C_{62}H_{112}N_{30}O_{25}Zn_4$, M_r = 1939.27, triclinic, space group $P\bar{1}$ (No. 2), T = 153 K, a = 14.5222(3) Å, b = 18.2326(4) Å, c = 19.7948(14) Å, α = 99.154(7)°, β = 104.171(7)°, γ = 113.428(8)°, V = 4464.9(6) $Å^3$, Z = 2, ρ_{calcd} = 1.442 g cm^{-3}, $2\theta_{max}$ = 89.0°, R = 0.1222 [for 4587 reflections with $I > 2\sigma(I)$], Rw = 0.3299 (for 6896 reflections), GOF = 0.922. CCDC 796371 contains the supplementary crystallographic data for the paper. These data can be obtained free of charge from The Cambridge Crystallographic Data Centre via www.ccdc.cam.ac.uk/data_request/cif.

Crystallographic Study of $3\cdot 8NO_3^-\cdot 4I^-\cdot 31H_2O$. A blue block crystal (0.15 × 0.13 × 0.10 mm) was obtained after slow evaporation of an aqueous solution of $3\cdot 8NO_3^-\cdot 4I^-\cdot 31H_2O$ over a period of 1 week. The results of elemental analysis suggested that 8 nitrate anions and 31 waters were contained in an asymmetric unit. However, only 4.932 nitrates and 8.540 waters could be located, in which the residual ones are supposed to be contained in the voids of 1743 $Å^3$ in the crystal and heavily disordered. Crystal data: $C_{124}H_{224.266}Cu_4I_4N_{56.932}O_{42.929}Zn_8$, M_r = 4484.50, triclinic, space group $P\bar{1}$ (No. 2), T = 93 K, a = 16.1372(3) Å, b = 17.1272(3) Å, c = 41.600(3) Å, α = 80.048(6)°, β = 87.810(7)°, γ = 63.549(5)°, V = 10129.3(9) $Å^3$, Z = 2, ρ_{calcd} = 1.470 g cm^{-3}, $2\theta_{max}$ = 136.6°, R = 0.1091 [for 22 149 reflections with $I > 2\sigma(I)$], Rw = 0.3380 (for 35 454 reflections), GOF = 1.146. CCDC 796372 contains the supplementary crystallographic data for this paper. These data can be obtained free of charge from The Cambridge Crystallographic Data Centre via www.ccdc.cam.ac.uk/data_request/cif.

Potentiometric pH Titrations. The preparation of the test solutions and the method used for calibration of the electrode system (potentiometric automatic titrator AT-400 and auto piston buret APB-410, Kyoto Electronics Manufacturing Co., Ltd.) with a Kyoto Electronics Manufacturing Co., Ltd., combination pH electrode 98100C171 have been described previously.[9−12] All of the titration solutions (50 mL) were maintained under an argon (>99.999% purity) atmosphere. The theoretical pH values corresponding to pH_1 and pH_2 were calculated as $pH_1' = 2.481$ and $pH_2' = 11.447$ using K_W ($=a_{H^+}a_{OH^-}$) = $10^{-14.00}$, K_W' ($=[H^+][OH^-]$) = $10^{-13.79}$, and f_{H^+} = 0.825. The corrected pH values ($-\log a_{H^+}$) were obtained using the following equations: $a = (pH_2' - pH_1')/(pH_2 - pH_1)$; $b = pH_2' - apH_2$; pH = a(pH-meter reading) + b. Potentiometric pH titrations were carried out with I = 0.10 ($NaNO_3$) at 25.0 ± 0.1 °C under an argon (>99.999% purity) atmosphere, and at least two independent titrations were always performed. Deprotonation constants and complexation constants K (defined in the text) were determined by means of the program *BEST*.[17] The pH σ-fit values defined in the program are smaller than 0.02. The obtained constants containing a term of $[H^+]$ were converted to corresponding mixed constants using $[H^+] = a_{H^+}/f_{H^+}$. The species distribution values (%) versus the pH (=$-\log a_{H^+}$) were obtained using the program *SPE*.[17]

Kinetics of MNP Hydrolysis. The kinetics of hydrolysis of MNP by **3** were measured by the initial slope method (following an increase in the absorption of released NP at 400 nm) in an aqueous solution at 37.0 ± 0.5 °C.[5e] Given amounts of a stock solution of **3** in an aqueous solution were added to the buffer [e.g., 10 mM buffer with I = 0.1 ($NaNO_3$)] in the cuvette at 37 °C (acetate for pH 5.0, MES for pH 6.0 and 6.5, HEPES for pH 7.0 and 7.4, EPPS for pH 8.0, CHES for pH 9.0, and CAPS for pH 10.0). After stirring for 5 min, the substrate was added to the sample solutions and the increase in the absorbance at 400 nm was monitored (ε_{400} values of NP are 1.21 × 10^3 M^{-1} cm^{-1} at pH 6.0, 5.00 × 10^3 M^{-1} cm^{-1} at pH 6.5, 1.00 × 10^4 M^{-1} cm^{-1} at pH 7.0, 1.35 × 10^4 M^{-1} cm^{-1} at pH 7.4, 1.70 × 10^4 M^{-1} cm^{-1} at pH 8.0, 1.78 × 10^4 M^{-1} cm^{-1} at pH 9.0, and 1.86 × 10^4 M^{-1} cm^{-1} at pH 10.0).[5e] For hydrolysis at pH 5−10, the hydrolysis products were also analyzed by HPLC using a reverse-phase column (Mightysil RP-4 GP 250-4.6; 5 μm; 250 × 4.6 mm i.d.; Kanto Chemical, Japan). The yields of NP were determined based on the working curve using uridine (U) as an external reference, a given amount of which was added to the reaction mixture (see Figure S8 in the Supporting Information). The HPLC separations were carried out with continuous eluent MeOH:1 mM HEPES (pH 7.4) = 5:95 (flow rate 1.0 mL min^{-1}) at room temperature. A total of 10 μL of each reaction mixture was injected into the HPLC system for analysis and analyzed at 254 nm. The initial hydrolysis rate (V_0) and k_{obs} values for **3** and AP were calculated from the decay slope (NP release rate/$[H\cdot MNP^- + MNP^{2-}]$), and their V_{max}, k_{cat}, and K_m values were determined by Lineweaver−Burk plots shown in Figure 8. The K_i values of the inhibitors (HPO_4^{2-}, amastatin, and captopril) were determined by the Dixon plots (data not shown). The k_{cat} and K_m values for AP were calculated from V_{max} using the unit values [mg of protein mL^{-1} and units (mg of protein)$^{-1}$] described in the product sheets attached with the purchased AP and the reported values for a dimer molecular weight of AP (9.4×10^4).[18]

RESULTS AND DISCUSSION

Crystal Structure of the 2:2 Complex of 1 and CA^{2-} (2) and the 4:4:4 Complex of 1, CA^{2-}, and Copper (3). Fine colorless crystals of the 2:2 complex, $[(Zn_2L)_2(CA^{2-})_2]^{4+}$ (**2**), of **1**[10c] and CA^{2-} (including 4 NO_3^- and 15 H_2O) were obtained by slow evaporation of a 1:1 mixture of **1** and CA in an aqueous solution at pH 7.4 with I = 0.1 ($NaNO_3$) at room temperature. The results of X-ray crystal structure analysis (Figure 1) showed a sandwich-like structure stabilized by four N(CA)−Zn^{2+} coordination bonds[12a] and π−π-stacking interactions between two bpy units (Figure 1b), in which two pyridine rings have a trans

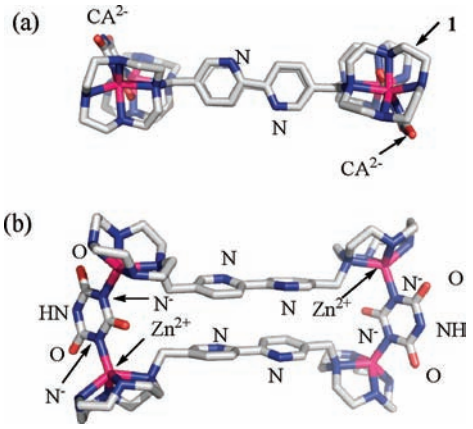

Figure 1. X-ray crystal structures of **2** (stick models): top view (a); side view (b). The averaged N(CA)−Zn^{2+} is 1.97 Å.

configuration in the solid state (Figure 1a).[19] Typical crystal structural parameters of **2** are listed in Table 1, and its ORTEP drawing is presented in Figure S1 in the Supporting Information.

The addition of 2 equiv of Cu ions [$Cu(NO_3)_2$, CuI, or CuBr] to a neutral aqueous solution of **2** gave a pale-blue solution, from which blue crystals were obtained. Its X-ray crystal structure analysis indicated a 2:4 assembly of **2** and Cu, namely, a 4:4:4 complex of **1**, CA^{2-}, and Cu, as shown in Figure 2 ($\{(Zn_2L)_4(CA^{2-})_4[Cu_2(OH)_2]_2\}^{12+}$, **3**), where the carbons are gray, nitrogens blue, oxygens red, iodines green, zincs pink, and coppers orange (the ORTEP drawing of **3** is shown in Figure S2 in the Supporting Information). This structure is stabilized by N^-−Zn^{2+} coordination bonds between Zn^{2+} and CA^{2-}, π−π stacking between bpy units (Figure 2a,b), and hydrogen bonds between two CA^{2-} (see Figure 2c). Importantly, **3** contains two μ-$Cu_2(OH)_2$ units in the center of the structure (Figure 2a,d), and each copper has a square-pyramidal structure including one water molecule (or I^-) at the apical position. The Cu−Cu and O−O distances in one μ-$Cu_2(OH)_2$ unit are ca. 2.9 and 2.6 Å, respectively, and the distances between two Cu ions of the μ-$Cu_2(OH)_2$ upside and downside are 4.7 Å (Figure 2d). It is likely that Cu^{2+}-bound I^- in the crystal is replaced by H_2O in an aqueous solution. The supermolecule **3** has a twisted chiral structure, resulting from unsymmetrical complementary hydrogen bonding between two CA^{2-} units, whose distances are 2.8−3.2 Å, as shown in Figure 2c,d (see also movie S1 in the Supporting Information). The exterior of **3** may be schematically represented as a twisted rectanglar form, the size of which is about 1.9 nm in length × 1.3 nm in width × 1.1 nm in height (Figure 2a,b).

Complexation Behaviors of 1 (Zn_2L)$^{4+}$ with CA^{2-} in Aqueous Solutions Determined by Potentiometric pH and UV/Vis Titrations. Evidence for the 2:2 (*n*:*n*) complexation of **1** and CA^{2-} in an aqueous solution was also supported by ^{1}H NMR (Figure S3 in the Supporting Information), potentiometric pH (typical potentiometric pH titration curves are shown in Figure S4 in the Supporting Information), and UV/vis spectrophotometric titrations. From the potentiometric pH titration, the pK_a values of two Zn^{2+}-bound waters of **1** (defined by eqs 1 and 2) were determined to be 7.2 ± 0.1, and 7.8 ± 0.1. The pK_a values of CA defined by eqs 3−5 were determined to be 6.9 ± 0.1, 10.9 ± 0.1, and >12, as previously reported.[12a]

Table 1. Representative Parameters of Crystal Structure Analyses of $2\cdot4NO_3^-\cdot15H_2O$ and $3\cdot8NO_3^-\cdot4I^-\cdot31H_2O$[a]

	$2\cdot4(NO_3^-)\cdot15H_2O$	$3\cdot8(NO_3^-)\cdot4(I^-)\cdot31H_2O$.[b]
empirical formula	$C_{62}H_{112}N_{30}O_{25}Zn_4$	$C_{124}H_{224.266}N_{56.932}O_{42.929}Cu_4Zn_8I_4$[b]
M_r	1939.27	4484.50
cryst syst	triclinic	triclinic
space group	$P\bar{1}$ (No. 2)	$P\bar{1}$ (No. 2)
a (Å)	14.5222(3)	16.1372(3)
b (Å)	18.2326(4)	17.1272(3)
c (Å)	19.7948(14)	41.600(3)
α (deg)	99.154(7)	80.048(6)
β (deg)	104.171(7)	87.810(7)
γ (deg)	113.428(8)	63.549(5)
V (Å^3)	4464.9(6)	10129.3(9)
Z	2	2
ρ_{calc} (g cm^{-3})	1.442	1.470
R	0.1222	0.1095
R_w	0.3299	0.3380
no. of reflns	6896	35 454
used for least squares	4717	19 080
GOF	0.922	1.146
F(000)	2028.00	4556.44
μ (mm^{-1})	1.954	6.894

[a] The structures were solved by direct methods (Rigaku & RAC07) and refined using least-squares techniques (*SHELXS97*). [b] See ref 16 and Table S6 in the Supporting Information.

$$Zn_2L\cdot(3-i)H_2O\cdot(i-1)HO^- \rightleftarrows Zn_2L\cdot(2-i)H_2O\cdot iHO^- + H^+ \quad (i = 1, 2) \tag{1}$$

$$K_{ai} = [Zn_2L\cdot(2-i)H_2O\cdot iHO^-]a_{H^+}/[Zn_2L\cdot(3-i)H_2O\cdot(i-1)HO^-] \tag{2}$$

$$CA \rightleftarrows CA^- + H^+: \quad K_{a1} = [CA^-]a_{H^+}/[CA] \tag{3}$$

$$CA^- \rightleftarrows CA^{2-} + H^+: \quad K_{a2} = [CA^{2-}]a_{H^+}/[CA^-] \tag{4}$$

$$CA^{2-} \rightleftarrows CA^{3-} + H^+: \quad K_{a3} = [CA^{3-}]a_{H^+}/[CA^{2-}] \tag{5}$$

Analysis of the potentiometric pH titration curve (Figure S4 in the Supporting Information) of a mixture of 0.5 mM **1** (Zn_2L) and 0.5 mM CA in an aqueous solution at 25 °C with I = 0.1 ($NaNO_3$) gave the intrinsic and apparent 2:2 complexation constants K_s(**2**) and K_{app}(**2**) (defined by eqs 6−13 and Scheme 2) of $10^{17.2\,\pm\,2.0}$ M^{-3} at pH 7.4. Figure 3 displays a speciation diagram of possible eight species: $Zn_2L(H_2O)_2$ [(**1a**)$^{4+}$], $Zn_2L(OH^-)_2$ [(**1c**)$^{2+}$], CA, CA^-, CA^{2-}, and $[(Zn_2L)_2(CA^{2-})_2]$ - [(**2a**)$^{4+}$, (**2b**)$^{3+}$, and (**2c**)$^{2+}$] as a function of the pH at 25 °C with I = 0.1 ($NaNO_3$), which shows that **2** is quantitatively formed at pH 6.5−8 when $[Zn_2L]_{total} = [CA]_{total}$ = 0.5 mM. Analysis of the potentiometric pH titration curve (c) in Figure S4 of the Supporting Information implied that the remaining imide protons of **2** (indicated by hollow arrows in Scheme 2) are deprotonated to give (**2b**)$^{3+}$ and (**2c**)$^{2+}$ species (indicated by

dx.doi.org/10.1021/ic201072q |*Inorg. Chem.* 2011, 50, 10113–10123

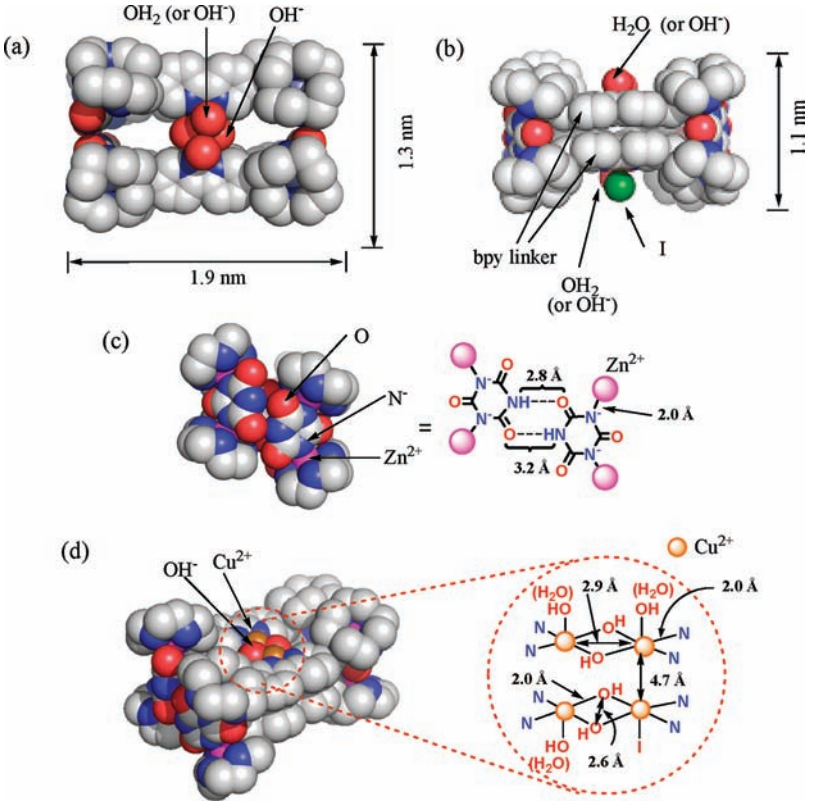

Figure 2. (a) Top view and (b) side view of **3** (space-filling models). Pink, orange, gray, blue, red, and green atoms are Zn^{2+}, Cu^{2+}, C, N, O, and I, respectively. (c) Side view of **3** from building unit CA^{2-} showing hydrogen bonding between two CA^{2-}. (d) Diagonal view of **3**, in which copper-coordinated H_2O (and I^-) are omitted. In the dashed circle, the crystal diagram shows representative coordination bond lengths in the μ-$Cu_2(OH)_2$ center of **3**. All external NO_3^- anions and H_2O molecules are omitted for clarity. The averaged lengths of the coordination bonds and hydrogen bonds are indicated in parts c and d.

eqs 7 and 8), as discussed in our previous paper.[12a]

$$2(Zn_2L)_{total} + 2(CA)_{total} \rightleftarrows [(Zn_2L)_2(CA^{2-})_2\ (\mathbf{2a})] \quad (6)$$

$$[\mathbf{2a}]^{4+} \rightleftarrows [(Zn_2L)_2(CA^{2-})(CA^{3-})\ (\mathbf{2b})]^{3+} + H^+ \quad (7)$$

$$[\mathbf{2b}]^{3+} \rightleftarrows [(Zn_2L)_2(CA^{3-})_2\ (\mathbf{2c})]^{2+} + H^+ \quad (8)$$

$$K_s(\mathbf{2}) = [\mathbf{2a}]/[Zn_2L\cdot 2H_2O\ (\mathbf{1a})]^2[CA^{2-}]^2 \quad (M^{-3}) \quad (9)$$

$$K_{app}(\mathbf{2}) = \{[(Zn_2L)_2(CA^{2-})_2]_{total}\}/[(Zn_2L)_{total}]^2[CA^{2-}]^2 \quad (M^{-3}) \quad (10)$$

$$[(Zn_2L)_{total}] = [Zn_2L\cdot 2H_2O\ (\mathbf{1a})] + [Zn_2L\cdot H_2O\cdot HO^-\ (\mathbf{1b})] + [Zn_2L\cdot 2HO^-\ (\mathbf{1c})] \quad (11)$$

$$[CA_{total}] = [CA] + [CA^-] + [CA^{2-}] \quad (12)$$

$$\{[(Zn_2L)_2(CA^{2-})_2]_{total}\} = [\mathbf{2a}] + [\mathbf{2b}] + [\mathbf{2c}] \quad (13)$$

UV/vis titrations of **1** with CA were carried out at pH 7.4 (10 mM HEPES) with $I = 0.1$ ($NaNO_3$)) at 25 °C. As shown in Figure 4, uncomplexed **1** (80 μM) has an absorption maximum (λ_{max}) at 289 nm, which decreased slightly upon the addition of CA, reaching a plateau at an *n*:*n* ratio, as shown in the inset, suggesting a 2:2 self-assembly of **1** with CA^{2-}, as evidenced by the X-ray crystal structure shown in Figure 1.

Complexation Behaviors of 2 with Cu^{2+} in Aqueous Solutions Studied by UV/Vis Titrations. UV/vis titrations of **2** (40 μM) with $Cu(NO_3)_2$ or CuBr induced a red shift from 287 to 309 nm, which reached a plateau at 2.0 equiv versus **2** (Figure 5a), indicative of the quantitative formation of **3** at micromolar-order concentrations. At the same time, an increase in the absorbance of **2** at ca. 650 nm was observed upon the addition of Cu^{2+} [$Cu(NO_3)_2$] or Cu^+ (CuBr), as shown in Figure 5b, corresponding to the μ-$Cu_2(OH)_2$ core, as has been reported for dinuclear copper(II) enzymes such as met-tyrosinase and oxy-hemocyanin,[20] indicating that **3** is quantitatively formed not only in the solid state but also in an aqueous solution. When CuBr was added to **2**, almost the same spectral change was observed, suggesting that Cu^+ is autooxidized to Cu^{2+} in situ to form the μ-$Cu_2(OH)_2$ structure in **3**. A thermal study, followed by UV/vis spectra, indicated that **3** undergoes a reversible structural change at temperatures below 50 °C and an irreversible change occurs at above 50 °C (see Figure S5 in the Supporting Information).[21,22]

Hydrolysis of MNP by 3. The central μ-$Cu_2(OH)_2$ cores of **3** disclosed by the X-ray structure resemble the catalytic centers of dinuclear metalloenzymes such as AP and KBPAP. Indeed, **3** (10 μM) accelerates the selective hydrolysis of MNP (100 μM), in an aqueous solution at pH 7.4 [10 mM HEPES with $I = 0.1$ ($NaNO_3$)] and 37 °C. As shown in Figure 6a, an increase in the

dx.doi.org/10.1021/ic201072q |*Inorg. Chem.* 2011, 50, 10113–10123

Scheme 2. Proposed Scheme for 2:2 Complexation of 1 (Zn_2L) and CA[a]

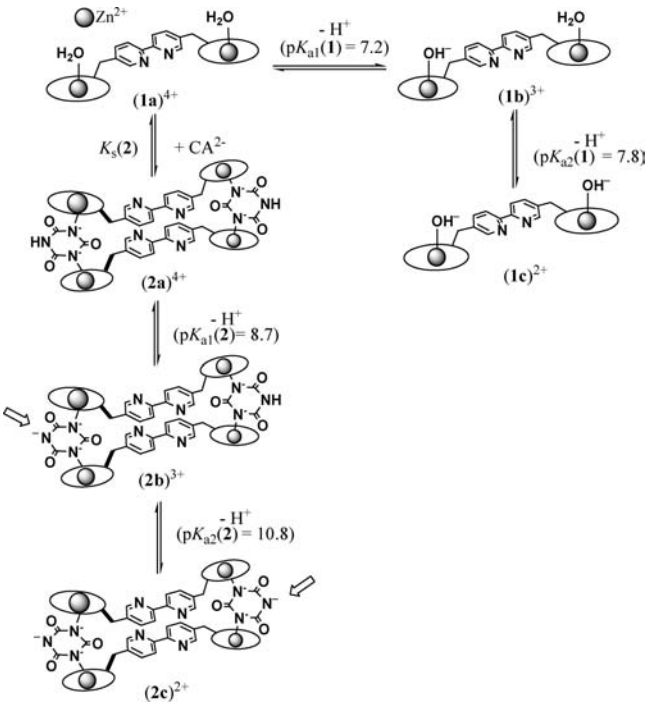

[a] Hollow arrows indicate the deprotonated imide sites in the 2:2 complex **2**.

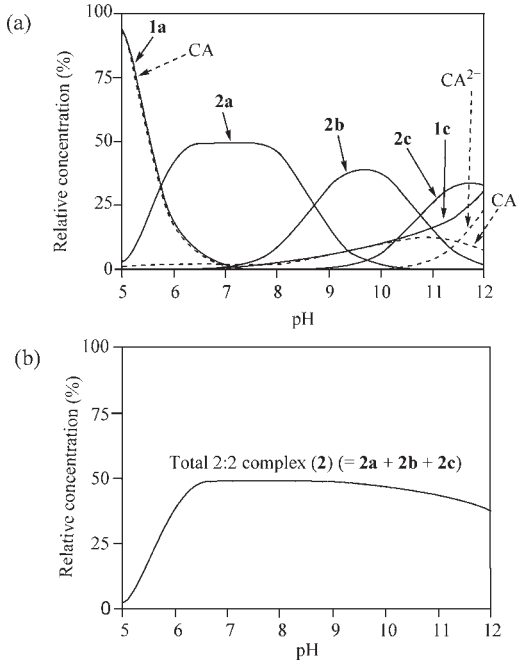

Figure 3. (a) Speciation diagram for species in a 1:1 mixture of **1** and CA at [**1**] = [CA] = 0.5 mM at pH 5−12, as defined by eqs 3−13. The species less than 5% [$(\mathbf{1b})^{3+}$] is omitted for clarity. (b) Speciation diagram of the total 2:2 complex (**2a** + **2b** + **2c**) in the pH range of 5−12 at [**1**] = [CA] = 0.5 mM.

absorbance at 400 nm was observed, corresponding to the formation of NP (ε_{400} = 1.35 × 10^4 M^{-1} cm^{-1} at pH 7.4).[5e] On the other hand, negligible or very slow hydrolysis of MNP

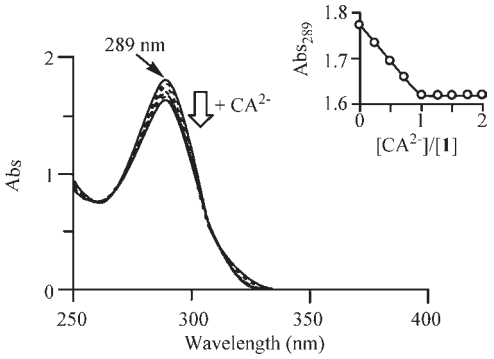

Figure 4. UV spectral change of **1** (80 μM) upon the addition of CA at pH 7.4 [10 mM HEPES with I = 0.1 ($NaNO_3$)] at 25 °C. The inset shows the decrease in ε_{289}.

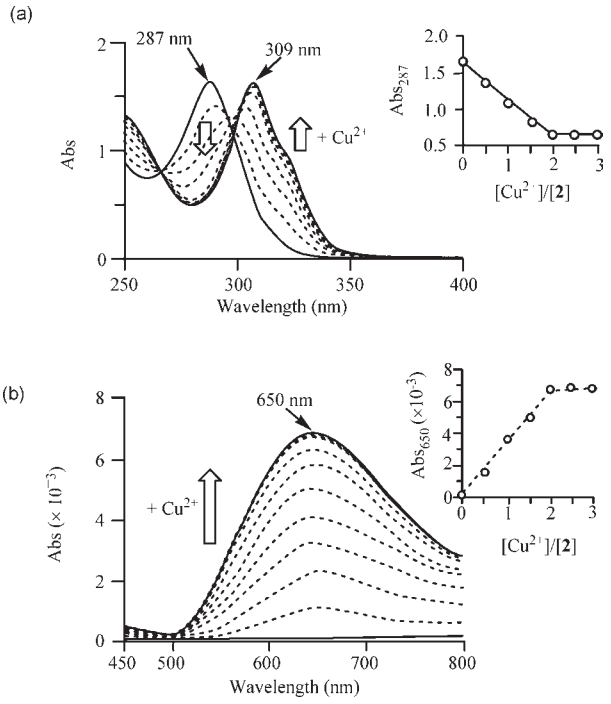

Figure 5. (a) UV/vis spectral change of a mixture of **2** (40 μM) upon the addition of Cu^{2+}. The inset shows the decrease in ε_{287} upon increasing concentrations of Cu^{2+}. (b) UV spectral change of **2** (40 μM) at 650 nm upon the addition of Cu^{2+}. The inset shows the increase in ε_{650} upon increasing ratio of Cu^{2+} versus **2**.

occurred in the presence of **1** alone, CA alone, **2** alone, Cu^{2+} alone, or $Cu(bpy)_2$ (4−100 μM). These results indicate that all of the three components, **1**, CA^{2-}, and Cu^{2+}, are required for the hydrolysis of MNP. More interestingly, it was found that the MNP hydrolysis proceeds over 30% yield (ca. 35% after 7 days, as shown in Figure 6b). On the basis of the assumption that two μ-$Cu_2(OH)_2$ units (20 μM = 20% of MNP) in **3** (10 μM) function independently, it has been suggested that **3** works as a catalyst for the hydrolysis of MNP. It is reported that the half-life of hydrolysis of a monoalkyl phosphate dianion such as mono(neopentyl) phosphate in wet cyclohexane is ca. 10^{11} years at 25 °C.[23] Therefore, the considerable acceleration of MNP hydrolysis by **3** is noteworthy.

dx.doi.org/10.1021/ic201072q |*Inorg. Chem.* 2011, 50, 10113–10123

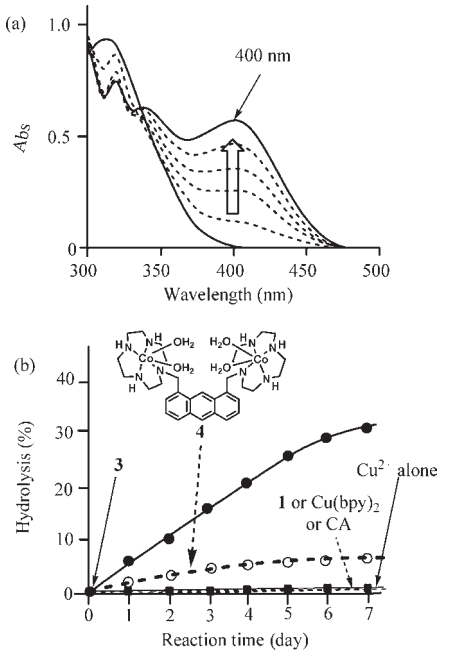

Figure 6. Hydrolysis of MNP by **3** at pH 7.4 [10 mM HEPES with I = 0.1 ($NaNO_3$)] and 37 °C. (a) UV/vis spectral change of the aqueous solution of MNP (100 μM) in the presence of **3** (10 μM). (b) Time course for the hydrolysis yield (produced NP) by **3** (bold curve with closed circles), **1**, $Cu(bpy)_2$ complex, CA [plain curve for **1**, $Cu(bpy)_2$, and CA], Cu^{2+} (closed circles), and Co_2(anthracene) complex **4** (bold dashed curve with open circles).

The results of screening various metal cations (Zn^{2+}, Co^{2+}, Ni^{2+}, Mn^{2+}, Fe^{2+}, and Fe^{3+}) indicated that Cu^{2+} is essential for the hydrolytic activity of **3** (Figure S6 in the Supporting Information). Negligible hydrolytic activity of **3** was observed in the hydrolysis of TNP, BNP, and carboxylic acid derivatives such as NA and Leu-NA. Bis(Co^{3+}-cyclen)anthracene (**4**; 10 mol %) reported by Vance and Czarnik[5d] accelerated the hydrolysis of MNP but not in a catalytic manner at pH 7.4 under our experimental conditions (Figure 6b), possibly because of complexation with inorganic phosphate (HPO_4^{2-}), a hydrolysis product.

The hydrolysis yields of MNP (chemical yields of the produced NP) by **3** in the pH range 5−10 (**3** is stable at pH 6−10, as shown in Figure S7 in the Supporting Information) were also monitored by HPLC, in which the concentrations of the produced NP at given reaction times were determined in comparison to that of an external reference, uridine (the retention times of MNP, NP, and uridine are 2, 20, and 6 min; see Figure S8 in the Supporting Information). Figure 7 is the pH profile showing that the highest hydrolysis yield ([NP produced in the presence of **3**] − [NP produced in the absence of **3**]) was obtained at pH 7.4.

A plot of the initial hydrolysis rate (V_0) versus [MNP] at [**3**] = 10 μM and a plot of V_0 versus [**3**] at [MNP] = 500 μM (Figure S9a,b in the Supporting Information) indicate that MNP hydrolysis by **3** follows the Michaelis−Menten scheme.[24] From the Lineweaver−Burk plot displayed in Figure 8a, V_{max} (the maximum velocity in the NP production from MNP promoted by **3**, μM min^{-1}) and K_m (Michaelis constant, M) values for **3** (10 μM) were determined to be (9.5 ± 0.2) × 10^{-3} μM min^{-1} and 470 ± 20 μM, as summarized in Table 2. This K_m value may be supported by the thermodynamic K_d values obtained by UV/vis titrations of **3** with phenyl phosphate (used instead of MNP),

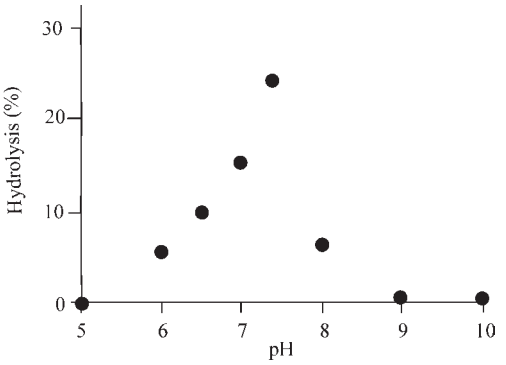

Figure 7. pH−rate profile for the **3**-catalyzed hydrolysis of MNP in a 10 mM buffer (pH 5−10) after reactions for 5 days (analyzed by HPLC, as displayed in Figure S8 in the Supporting Information). Hydrolysis yields were calculated based on the concentration of NP produced by **3**-catalyzed hydrolysis of MNP (=[NP produced in the presence of **3**] − [NP produced in the absence of **3**]).

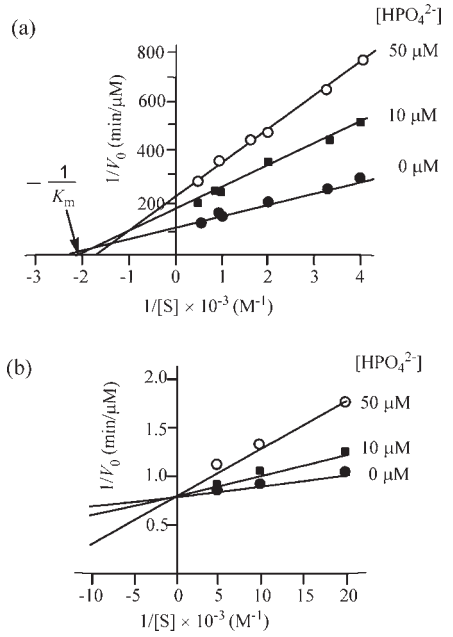

Figure 8. Lineweaver−Burk plot for the hydrolysis of MNP catalyzed by **3** (a) and AP (b) in the absence and presence of HPO_4^{2-} (0, 10, and 50 μM) in 10 mM HEPES (pH 7.4) at 37 °C.

as shown in Figure S10a in the Supporting Information.[25] The k_{cat} value defined by eq 14 was calculated to be (9.5 ± 0.2) × 10^{-4} min^{-1}.

$$k_{cat} = V_{max}/[\text{catalyst}](\text{catalyst} = \mathbf{3} \text{ or AP}) \quad (14)$$

It is known that HPO_4^{2-}, a hydrolysis product of MNP, inhibits AP (product inhibition).[2,18] In Figure 6b, it was indicated that the **3**-catalyzed MNP hydrolysis velocity becomes slower as the reaction proceeds, possibly because of product inhibition. Therefore, MNP hydrolysis in the presence of HPO_4^{2-} was carried out (the initial [HPO_4^{2-}] values were 0, 10, and 50 μM). The Lineweaver−Burk plot in Figure 8a suggests that HPO_4^{2-} exhibits mixed-type inhibition[24] versus **3** and the K_i was estimated to be ca. 70 μM (Table 2). This approximate K_i of HPO_4^{2-} is roughly supported by the UV/vis titrations of **3** with

dx.doi.org/10.1021/ic201072q |Inorg. Chem. 2011, 50, 10113–10123

Table 2. Kinetic Parameters (V_{max}, k_{cat}, and K_m) for Hydrolysis of MNP by Supramolecular Catalyst 3 and AP and K_i Values of HPO_4^{2-} versus These Catalysts in 10 mM HEPES (pH 7.4) with I = 0.1 ($NaNO_3$) at 37 °C

	V_{max} (μM min^{-1})	k_{cat} (min^{-1})	K_m (μM)	K_i of HPO_4^{2-} (μM)
3	$(9.5 \pm 0.2) \times 10^{-3}$ [a]	$(9.5 \pm 0.2) \times 10^{-4}$ [a]	470 ± 20 [a]	ca. 70 [a] (mixed type)
AP	1.3 ± 0.1 [a]	$(2.4 \pm 0.2) \times 10^{3}$ [a,b]	7 ± 4 [a]	3 ± 1 [a] (competitive)
		$(2.1 \pm 0.1) \times 10^{3}$ [c]	3.7 ± 0.3 [c]	7.7[c]

[a] Determined in this work. [b] The k_{cat} value for AP was calculated from V_{max} by using a molecular weight of 9.4×10^4 as the AP dimer, according to ref 18. [c] From ref 18 [at pH 8.0 in 0.1 M MOPS with I = 0.1 (NaCl)].

HPO_4^{2-}, which gave the thermodynamic K_d values of ca. 80 μM for **3**-HPO_4^{2-} complexation (Figure S10b in the Supporting Information). The MNP hydrolysis at [MNP] = 1 mM, which is greater than these K_i and K_m values, somehow improved the catalytic turnover number (CTN) up to ca. 3−4 (Figure S11 in the Supporting Information).

For comparison, the kinetic parameters of MNP hydrolysis by AP from *E. coli* (EC 3.1.3.1) are also listed in Table 2. From the Lineweaver−Burk plot of AP (Figure 8b), the K_i value of HPO_4^{2-} versus AP was determined to be 3 ± 1 μM, which agrees well with the reported value (HPO_4^{2-} is a competitive inhibitor of AP).[18] The effects of amastatin, an inhibitor of leucine aminopeptidase (dizinc peptidase), and captopril, an inhibitor of angiotensin−converter−enzyme (monozinc peptidase), were negligible on the MNP hydrolysis by **3** and AP (K_i > 1.0 mM).

Proposed Mechanism of MNP Hydrolysis by 3. The MNP hydrolysis by 4:4:4 supramolecular complex **3** was carried out in H_2O (pH 7.4) and D_2O (p*D* 7.4) in order to check the isotope effect. As shown in Figure S12 in the Supporting Information, the MNP hydrolysis in D_2O was reduced to about half of that in H_2O, strongly indicating that Cu^{2+}-bound H_2O (or OH^-) is involved in the rate-determining steps in the MNP hydrolysis catalyzed by **3**.

Considering the experimental results described above and the fact that only MNP is hydrolyzed together with the proposed mechanisms for dinuclear metal hydrolases,[3] three possible reaction mechanisms of **3**-catalyzed MNP hydrolysis are proposed, as shown in Scheme 3. The first assumption includes the following: (i) the dianion form of MNP (MNP^{2-}) bridges two Cu^{2+} ions in the catalytic μ-$Cu_2(OH)_2$ center of **3** (**5** ⇄ **6** in Scheme 3;[26] the pK_{a2} value of MNP is 5.2);[5e,27] (ii) the hydroxyl anion in the μ-$Cu_2(OH)_2$ unit attacks the P atom of MNP to facilitate cleavage of the ester bond and release NP (**6** → **7** → **8**);[2f] (iii) recoordination of the H_2O molecules to Cu ions then induces the release of HPO_4^{2-} with catalyst reactivation (**8** → **5**). However, this last step is presumably slow and is one of the rate-determining steps in the catalytic cycle as in the case of AP,[18] resulting in the low CTN (~4). The second scenario would include (i) the chelation of MNP^{2-} to one Cu^{2+} in the μ-$Cu_2(OH)_2$ unit (**5** → **9**) and (ii) the nucleophilic attack of the Cu^{2+}-bound OH anion to the phosphorus of MNP to give **11** via **10**. It is also likely that HPO_4^{2-} binds to two Cu^{2+} ions (**11**), resulting in inhibition of **3**. The third possibility would be MNP hydrolysis via the intermediate **12**, in which one of the oxyanions of MNP bridges two Cu^{2+} ions. The nucleophilic attack of the Cu^{2+}-bound OH^- would afford **8**, which is the same intermediate from **7**. These several hydrolysis routes and inhibition modes by HPO_4^{2-} (**8** and **11**) may explain the mixed-type inhibition suggested by the Lineweaver−Burk plot in Figure 8a.[28]

Sequential and Reversible Self-Assembly of 3. Most of the previously reported supramolecular complexes were synthesized prior to the reactions. Because the formation of **3** is reversible, the effect of the mixing sequence on the hydrolytic activity was examined. A mixture of **1** and Cu^{2+} (or Cu^+) (without CA^{2-}) induced negligible hydrolysis of MNP after 24 h and the addition

Scheme 3

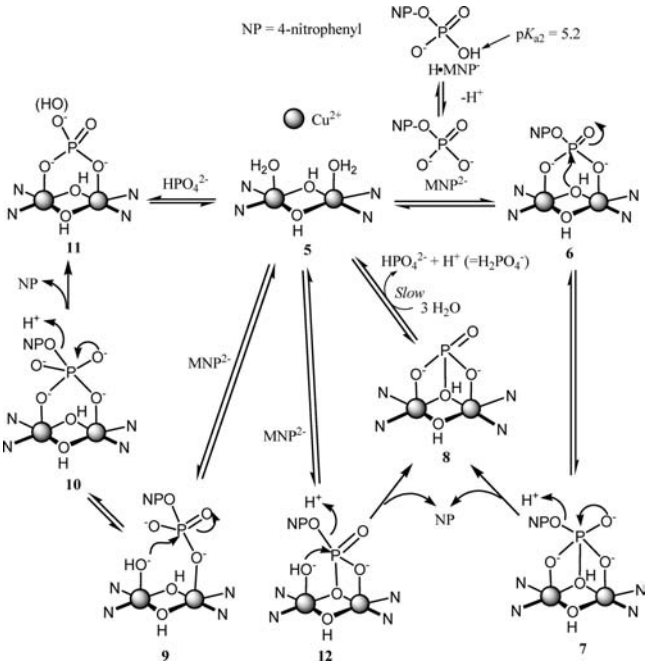

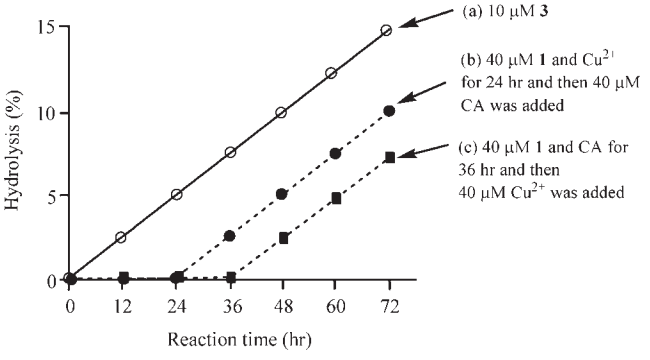

Figure 9. Effect of mixing order of the building modules of **3** on the hydrolysis of MNP (100 μM) in 100 mM HEPES [pH 7.4 with I = 0.1 ($NaNO_3$)] and 37 °C: (a) MNP hydrolysis in the presence of 10 μM **3**; (b) MNP hydrolysis in the presence of 40 μM **1** + 40 μM Cu^{2+} for 24 h and then 40 μM CA was added; (c) MNP hydrolysis in the presence of 40 μM **1** + 40 μM CA for 36 h and then 40 μM Cu^{2+} was added.

dx.doi.org/10.1021/ic201072q |*Inorg. Chem.* 2011, 50, 10113–10123

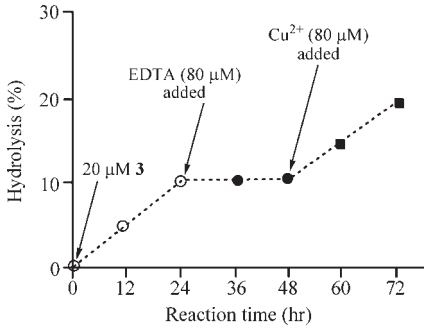

Figure 10. Effect of the addition of EDTA on the MNP hydrolysis by **3** in 100 mM HEPES [pH 7.4 with I = 0.1 ($NaNO_3$)] and 37 °C. After incubation of 100 μM MNP in the presence of 20 μM **3**, 80 μM EDTA was added to a reaction mixture to stop the MNP hydrolysis. The addition of 80 μM Cu^{2+} at 48 h restored the hydrolytic activity of **3**.

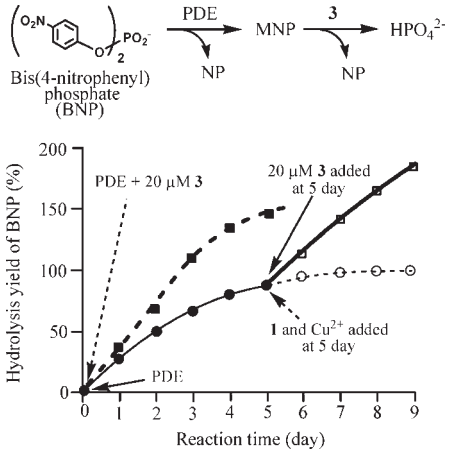

Figure 11. Hydrolysis of BNP (50 μM) by PDE (5×10^{-3} units mL^{-1}) for 5 days (with 20 μM EDTA) at pH 7.4 [10 mM HEPES with I = 0.1 ($NaNO_3$)] and 37 °C (plain curve with closed circles), followed by the addition of **3** (20 μM) (formed by in situ from 80 μM **1**, 80 μM CA, and 120 μM Cu^{2+}) (bold curve with open squares) or **1** and Cu^{2+} (80 μM) (dashed curve with open circles) for 4 days. A bold dashed curve (with closed squares) shows one-pot hydrolysis of BNP (50 μM) to NP and HPO_4^{2-} by PDE (5×10^{-3} units mL^{-1}) and **3** (20 μM) at pH 7.4 [10 mM HEPES with I = 0.1 ($NaNO_3$) and 20 μM EDTA] and 37 °C.

of CA initiated hydrolysis (curve b in Figure 9) at almost the same rate as that for curve a. Similarly, negligible evidence was found for the hydrolysis of MNP in the presence of only **1** and CA (closed squares), and the addition of Cu^{2+} (or Cu^{+}) after 36 h initiated the hydrolysis (curve c in Figure 9). These facts suggest that the formation of **3** from three molecular modules (**1**, CA^{2-}, and Cu^{2+}) takes place in a programmed fashion regardless of the mixing order of three molecules even in the presence of the substrate (MNP). This was also supported by UV/vis titrations of a mixture of **1** and Cu^{2+} with CA (see Figure S14 in the Supporting Information).

Moreover, the hydrolytic activity of **3** can be controlled by metal chelators such as ethylenediamine-*N*,*N*,*N*′,*N*′-tetraacetic acid (EDTA) or *N*,*N*,*N*′,*N*′-tetrakis(2-pyridylmethyl)methylenediamine. For example, the addition of EDTA (80 μM) to a mixture of MNP (100 μM) and **3** (20 μM) after incubation for 24 h stopped the MNP hydrolysis, and the addition of Cu^{2+} (80 μM) to this mixture restored the hydrolytic activity of **3** (Figure 10).

One-Pot Chemoenzymatic Hydrolysis of BNP to Inorganic Phosphate Using Phosphodiesterase and 3. Finally, we examined the two-step hydrolysis from BNP to NP by the combined use of **3** with PDE from *C. atrox* (EC 3.1.4.1), an enzyme that catalyzes the hydrolysis of BNP to MNP and not from MNP to NP, in the same reaction mixture. Hydrolysis of 50 μM BNP by PDE (5.0×10^{-3} units mL^{-1}) at pH 7.4 [10 mM HEPES with I = 0.1 ($NaNO_3$)] and 37 °C proceeded ca. 95% after incubation for 5 days (plain curve and closed circles), and the successive addition of **3** (20 μM) to this reaction mixture and incubation for an additional 4 days resulted in ca. 180−190% production of NP based on the initial amount of BNP (bold curve in Figure 11). In contrast, the addition of only **1** and Cu^{2+} negligibly accelerated the hydrolysis of MNP (dashed curve). A bold dashed curve (with closed squares) in Figure 11 indicates that the hydrolysis of 50 μM BNP in the copresence of **3** (20 μM) and PDE (5.0×10^{-3} units mL^{-1}) resulted in ca. 145% release of NP, suggesting biocompatibility of **3** for the one-pot chemoenzymatic synthesis in an aqueous solution.

CONCLUSIONS

In conclusion, we successfully constructed the supramolecular catalyst **3**, which contains μ-$Cu_2(OH)_2$ center cores, mimicking the active centers of dimetallic phosphatases, by the quantitative 4:4:4 self-assembly of bis(Zn^{2+}-cyclen) complex **1** (Zn_2L) with CA^{2-} and Cu^{2+}, as confirmed by potentiometric pH, UV/vis spectrophotometric titrations, and X-ray crystallographic analyses. To our knowledge, **3** represents the first supramolecular phosphatase that is formed by self-assembly and selectively hydrolyzes a phosphate monoester catalytically under physiological conditions. Allthough the CTN is about 2−4, the considerable acceleration of MNP hydrolysis by **3** in an aqueous solution at neutral pH is noteworthy. These results should be useful in the future design of stable, biologically active, and biocompatible supramolecular catalysts.

ASSOCIATED CONTENT

Supporting Information. Figures S1−S14 and Tables S1−S6 and X-ray crystal structure data for the supramolecular complexes **2** and **3**. This material is available free of charge via the Internet at http://pubs.acs.org.

AUTHOR INFORMATION

Corresponding Author
*E-mail: shinaoki@rs.noda.tus.ac.jp.

ACKNOWLEDGMENT

This work was supported by the Grants-in-Aid from the Ministry of Education, Science and Culture in Japan (Grants 19659026, 22390005, and 22659005). S.A. and M.Z. are thankful for the grant and postdoctoral fellowship for foreign researchers from Japan Society for the Promotion of Science (JSPS; Grant 20-08451). We are thankful to Fukiko Hasegawa (Faculty of Pharmaceutical Sciences, Tokyo University of Science) and Dr. Yoshiyuki Itoh (JEOL, Japan) for measurement of the mass spectra of **2** and **3**.

REFERENCES

(1) (a) Woodgett, J. *Protein Kinase Functions, Frontiers in Molecular Biology*; Oxford University Press: Oxford, U.K., 2000. (b) Denu, J. M.; Stuckey, J. A.; Saper, M. A.; Dixon, J. E. *Cell* **1996**, *87*, 361–364.

(2) (a) Averill, B. A. In *Comprehensive Coordination Chemistry II*; Que, L., Jr., Tolman, W. B., Eds.; Elsevier: Amsterdam, The Netherlands, 2003; Vol. 8, pp 641−676. (b) Christianson, D. W.; Cox, J. D. *Annu. Rev. Biochem.* **1999**, *68*, 33–57. (c) Vallee, B. L.; Auld, D. S. *Acc. Chem. Res.* **1993**, *26*, 543–551. (d) Auld, D. S. *Biometals* **2001**, *14*, 271–313. (e) Cleland, W. W.; Hengge, A. C. *Chem. Rev.* **2006**, *106*, 3252–3278. (f) Kimura., E. *Curr. Opin. Chem. Biol.* **2000**, *4*, 207–213. (g) Aoki, S.; Kimura, E. In *Comprehensive Coordination Chemistry II*; Que, L., Jr., Tolman, W. B., Eds.; Elsevier: Amsterdam, The Netherlands, 2003; Vol. 8, pp 601−640. (h) Weston, J. *Chem. Rev.* **2005**, *105*, 2151–2174. (i) Cotton, F. A.; Wilkinson, G. *Advances in Inorganic Chemistry: A Comprehensive Text*, 5th ed.; Wiley-VCH: New York, 1988; Vol. 1.

(3) For reviews, see: (a) Vahrenkamp, H. *Acc. Chem. Res.* **1999**, *32*, 589–596. (b) Suh, J. *Acc. Chem. Res.* **2003**, *36*, 562–570. (c) Garcia-Espana, E.; Diaz, P.; Llinares, J. M.; Bianchi, A. *Coord. Chem. Rev.* **2006**, *250*, 2952–2986. (d) Natale, D.; Mareque-Rivas, J. C. *Chem. Commun.* **2008**, 425–437. (e) Mewis, R. E.; Archibald, S. J. *Coord. Chem. Rev.* **2010**, *254*, 1686–1712. (f) Mitic, N.; Smith, S. J.; Neves, A.; Guddat, L. W.; Gahan, L. R.; Schenk, G. *Chem. Rev.* **2006**, *106*, 3345–2174.

(4) (a) Kaminskaia, N. V.; He, C.; Lippard, S. J. *Inorg. Chem.* **2000**, *39*, 3365–3373. (b) Jeung, C.-S.; Song, J. B.; Kim, Y.-H.; Suh, J. *Bioorg. Med. Chem. Lett.* **2001**, *11*, 3061–3064. (c) Ait-Haddoun, H.; Sumaoka, J.; Wiskur, S. L.; Folmer-Andersen, J. F.; Anslyn, E. V. *Angew. Chem., Int. Ed.* **2002**, *41*, 4013–4016. (d) Scarso, A.; Scheffer, U.; Göbel, M.; Broxterman, Q. B.; Kaptein, B.; Formaggio, F.; Toniolo, C.; Scrimin, P. *Proc. Natl. Acad. Sci. U.S.A.* **2002**, *99*, 5144–5149. (e) Humphry, T.; Forconi, M.; Williams, N. H.; Hengge, A. C. *J. Am. Chem. Soc.* **2004**, *126*, 11864–11869. (f) Knight, D. A.; Delehanty, J. B.; Goldman, E. R.; Bongard, J.; Streich, F.; Edwards, L. W.; Chang, E. L. *Dalton Trans.* **2004**, 2006–2011. (g) Jikido, R.; Shiraishi, H.; Matsufuji, K.; Ohba, M.; Furutachi, H.; Suzuki, M.; Okawa, H. *Bull. Chem. Soc. Jpn.* **2005**, *78*, 1795–1803. (h) Maldonado Calvo, J. A.; Vahrenkamp, H. *Inorg. Chim. Acta* **2005**, *358*, 4019–4026. (i) Maldonado Calvo, J. A.; Vahrenkamp, H. *Inorg. Chim. Acta* **2006**, *359*, 4079–4086. (j) Jiang, F.; Huang, L.; Meng, X.; Du, J.; Yu, X.; Zhao, Y.; Zeng, X. *J. Colloid Interface Sci.* **2006**, *303*, 236–242. (k) Sumaoka, J.; Chen, W.; Kitamura, Y.; Tomita, T.; Yoshida, J.; Komiyama, M. *J. Alloys Compd.* **2006**, *408*−*412*, 391–395. (l) Belousoff, M. J.; Duriska, M. B.; Graham, B.; Batten, S. R.; Moubaraki, B.; Murray, K. S.; Spiccia, L. *Inorg. Chem.* **2006**, *45*, 3746–3755. (m) Feng, G.; Mareque-Rivas, J. C.; Williams, N. H. *Chem. Commun.* **2006**, 1845–1847. (n) Feng, G.; Natale, D.; Prabaharan, R.; Mareque-Rivas, J. C.; Willaims, N. H. *Angew. Chem., Int. Ed.* **2006**, *45*, 7056–7059. (o) Perez Olmo, C.; Bohmerle, K.; Vahrenkamp, H. *Inorg. Chim. Acta* **2007**, *360*, 1510–1516. (p) Mancin, F.; Tecilla, P. *New J. Chem.* **2007**, *31*, 800–817. (q) Cartuyvels, E.; Absillis, G.; Parac-Vogt, T. N. *Chem. Commun.* **2008**, 85–87. (r) Takebayashi, S.; Shinkai, S.; Ikeda, M.; Takeuchi, M. *Org. Biomol. Chem.* **2008**, *6*, 493–499. (s) Bonomi, R.; Selvestrel, F.; Lombardo, V.; Sissi, C.; Polizzi, S.; Mancin, F.; Tonellato, U.; Scrimin, P. *J. Am. Chem. Soc.* **2008**, *130*, 15744–15756. (t) Taran, O.; Medrano, F.; Yatsimirsky, A. K. *Dalton Trans.* **2008**, 6609–6618. (u) Subat, M.; Woinaroschy, K.; Gerstl, C.; Sarkar, B.; Kaim, W.; Konig, B. *Inorg. Chem.* **2008**, *47*, 4661–4668. (v) Penkova, L. V.; Maciag, A.; Rybak-Akimova, E. V.; Haukka, M.; Pavlenko, V. A.; Iskenderov, T. S.; Kozlowski, H.; Meyer, F.; Fritsky, I. O. *Inorg. Chem.* **2009**, *48*, 6960–6971. (w) Piovezan, C.; Jovito, R.; Bortoluzzi, A. J.; Terenzi, H.; Fischer, F. L.; Severiono., P. C.; Pich, C. T.; Azzolini, G. G.; Peralta, R. A.; Rossi, L. M.; Neves, A. *Inorg. Chem.* **2010**, *49*, 2580–2582. (x) Bonomi, R.; Scrimin, P.; Mancin, F. *Org. Biomol. Chem.* **2010**, *8*, 2622–2626.

(5) (a) Seo, J. S.; Sung, N.-D.; Hynes, R. C.; Chin, J. *Inorg. Chem.* **1996**, *35*, 7472–7473. (b) Williams, N. H.; Lebuis, A.-M.; Chin, J. *J. Am. Chem. Soc.* **1999**, *121*, 3341–3348. (c) Williams, N. H.; Takasaki, B.; Wall, M.; Chin, J. *Acc. Chem. Res.* **1999**, *32*, 485–493. (d) Vance, D. H.; Czarnik, A. W. *J. Am. Chem. Soc.* **1993**, *115*, 12165–12166. (e) Koike, T.; Inoue, M.; Kimura, E.; Shiro., M. *J. Am. Chem. Soc.* **1996**, *118*, 3091–3099. (f) Hettich, R.; Schneider, H.-J. *J. Am. Chem. Soc.* **1997**, *119*, 5638–5647.

(6) For review, see: (a) Coon, M. M.; Rebek, J., Jr. *Chem. Rev.* **1997**, *97*, 1647–1668. (b) Fujita, M. *Molecular Self-Assembly Organic Versus Inorganic Approaches*; Springer: Berlin, 2000; Vol. 96. (c) Breit, B. *Angew. Chem., Int. Ed.* **2005**, *44*, 6816–6825. (d) Kleij, A. W.; Reek, J. N. H. *Chem.—Eur. J.* **2006**, *12*, 4218–4227. (e) Oshovsky, G. V.; Reinhoudt, D. N.; Verboom, W. *Angew. Chem., Int. Ed.* **2007**, *46*, 2366–2393. (f) Hannon, M. J. *Chem. Soc. Rev.* **2007**, *36*, 280–295. (g) van Leeuwen, P. W. N. M. *Supramolecular Catalysis*; Wiley-VCH: New York, 2008. (h) Koblenz, T. S.; Wassenaar, J.; Reek, J. N. H. *Chem. Soc. Rev.* **2008**, *37*, 247–262. (i) Suzuki, K.; Tominaga, M.; Kawano, M.; Fujita, M. *Chem. Commun.* **2009**, 1638–1640. (j) Northrop, B. H.; Zheng, Y.-R.; Chi, K.-W.; Stang, P. J. *Acc. Chem. Res.* **2009**, *42*, 1554–1563. (k) Leugn, K. C.-F.; Chak, C.-P.; Lo, C.-M.; Wong, W.-Y.; Xuan, S.; Cheng, C. H. K. *Chem.—Asian J.* **2009**, *4*, 364–381. (l) Yoshizawa, M.; Klosterman, J. K.; Fujita, M. *Angew. Chem., Int. Ed.* **2009**, *48*, 3418–3438. (m) Yoshizawa, M.; Fujita, M. *Bull. Chem. Soc. Jpn.* **2010**, *83*, 609–618. (n) Traboisi, A.; Khashab, N.; Fahrenbach, A. C.; Friedman, D. C.; Colvin, M. T.; Coti, K. K.; Benitez, D.; Tkatchouk, E.; Olsen, J.-C.; Belowich, M. E.; Carmielli, R.; Khatib, H. A.; Goddard, W. A.; Wasielewski, M. R.; Stoddart, J. F. *Nat. Chem.* **2010**, *2*, 42–49. (o) Meeuwissen, J.; Reek, J. N. H. *Nat. Chem.* **2010**, *2*, 615–621. (p) Ma, Z.; Moulton, B. *Coord. Chem. Rev.* **2011** (doi: 10.1016/j.ccr.2011.01.031).

(7) (a) Gibb, C. L. D.; Gibb, B. C. *J. Am. Chem. Soc.* **2004**, *126*, 11408–11409. (b) Slagt, V. F.; Kamaer, P. C. J.; van Leeuwen, P W. N. M.; Reek, J. N. H. *J. Am. Chem. Soc.* **2004**, *126*, 1526–1536. (c) Kuil, M.; Soltner, T.; van Leeuwen, P. W. N. M.; Reek, J. N. H. *J. Am. Chem. Soc.* **2006**, *128*, 11344–11345. (d) Neelakandan, P. P.; Hariharan, M.; Ramaiah, D. *J. Am. Chem. Soc.* **2006**, *128*, 11334–11335. (e) Nishioka, Y.; Yamaguchi, T.; Yoshizawa, M.; Fujita, M. *J. Am. Chem. Soc.* **2007**, *129*, 7000–7001. (f) Natarajan, A.; Kaanumalle, L. S.; Jockusch, S.; Gibb, C. L. D.; Gibb, B. C.; Turro, N. J.; Ramamurthy, V. *J. Am. Chem. Soc.* **2007**, *129*, 4132–4133. (g) Sawada, T.; Yoshizawa, M.; Sato, S.; Fujita, M. *Nat. Chem.* **2009**, *1*, 53–56. (h) Gianneschi, N. C.; Nguyen, S. T.; Mirkin, C. A. *J. Am. Chem. Soc.* **2005**, *127*, 1644–1645. (i) Lee, S. J.; Cho, S.-H.; Mulfort, K. L.; Tiede, D. M.; Hupp, J. T.; Nguyen, S. T. *J. Am. Chem. Soc.* **2008**, *130*, 16828–16829. (j) Murase, T.; Horiuchi, S.; Fujita, M. *J. Am. Chem. Soc.* **2010**, *132*, 2866–2867.

(8) (a) Merlau, M. L.; del Pilar Mejia, M.; Nguyen, S. T.; Hupp, J. T. *Angew. Chem., Int. Ed.* **2001**, *40*, 4239–4242. (b) Yoshizawa, M.; Tamura, M.; Fujita, M. *Science* **2006**, *312*, 251–254. (c) Leung, D. H.; Bergman, R. G.; Raymond, K. N. *J. Am. Chem. Soc.* **2006**, *128*, 9781–9797. (d) Leung, D. H.; Bergman, R. G.; Raymond, K. N. *J. Am. Chem. Soc.* **2007**, *129*, 2746–2747. (e) Fielder, D.; Leugn, D. H.; Raymond, K. N. *Science* **2007**, *316*, 85–88. (f) Iwasawa, T.; Hooley, R. J.; Rebek, J., Jr. *Science* **2007**, *317*, 493–496. (g) Brown, C. J.; Bergman, R. G.; Raymond, K. N. *J. Am. Chem. Soc.* **2009**, *131*, 17530–17531. (h) Pluth, M. D.; Bergman, R. G.; Raymond, K. N. *J. Org. Chem.* **2009**, *74*, 58–63. (i) Shultz, A. M.; Farha, O. K.; Hupp, J. T.; Nguyen, S. T. *J. Am. Chem. Soc.* **2009**, *131*, 4204–4205. (j) Lee, J. Y.; Farha, O. K.; Roberts, J.; Scheidt, K. A.; Nguyen, S. T.; Hupp, J. T. *Chem. Soc. Rev.* **2009**, *38*, 1450–1459. (k) Pignataro, L.; Lynikaite, B.; Cvengros, J.; Marchini, M.; Piarulli, U.; Gennari, C. *Eur. J. Org. Chem.* **2009**, 2539–2547. (l) Hastings, C. J.; Pluth, M. D.; Bergman, R. G.; Raymond, K. N. *J. Am. Chem. Soc.* **2010**, *132*, 6938–6940.

(9) (a) Shionoya, M.; Kimura, E.; Shiro, M. *J. Am. Chem. Soc.* **1993**, *115*, 6730–6737. (b) Koike, T.; Takashige, M.; Kimura, E.; Fujioka, H.; Shiro, M. *Chem.—Eur. J.* **1996**, *2*, 617–623. (c) Kimura, E.; Kikuta, E. *Prog. React. Kinet. Mech.* **2000**, *25*, 1–64. (d) Aoki, S.; Iwaida, K.; Hanamoto, N.; Kitamura, H.; Koike, T.; Kimura, E. *J. Am. Chem. Soc.* **2002**, *124*, 5256–5257. (e) Aoki, S.; Kimura, E. *Chem. Rev.* **2004**, *104*, 769–788. (f) Kitamura, M.; Nishimoto, H.; Aoki, K.; Tsukamoto, M.; Aoki, S. *Inorg. Chem.* **2010**, *49*, 5316–5327.

(10) (a) Aoki, S.; Kagata, D.; Shiro, M.; Takeda, K.; Kimura, E. *J. Am. Chem. Soc.* **2004**, *126*, 9129–9139. (b) Aoki, S.; Jikiba, A.; Takeda, K.; Kimura, E. *J. Phys. Org. Chem.* **2004**, *17*, 489–497. (c) Aoki, S.; Zulkefeli,

M.; Shiro, M.; Kohsako, M.; Takeda, K.; Kimura, E. *J. Am. Chem. Soc.* **2005**, *127*, 9129–9139.

(11) Itoh, S.; Kitamura, M.; Yamada, Y.; Aoki, S. *Chem.—Eur. J.* **2009**, *15*, 10570–10584.

(12) (a) Aoki, S.; Shiro, M.; Koike, T.; Kimura, E. *J. Am. Chem. Soc.* **2000**, *122*, 576–584. (b) Aoki, S.; Shiro, M.; Kimura, E. *Chem.—Eur. J.* **2002**, *8*, 929–939. (c) Aoki, S.; Zulkefeli, M.; Shiro, M.; Kimura, E. *Proc. Natl. Acad. Sci. U.S.A.* **2002**, *99*, 4894–4899. (d) Zulkefeli, M.; Sogon, T.; Takeda, K.; Kimura, E.; Aoki, S. *Inorg. Chem.* **2009**, *48*, 9567–9578.

(13) (a) Huang, W.; Zhu, H.-B.; Gou, S.-H. *Coord. Chem. Rev.* **2006**, *250*, 414–423. (b) Tranchemontagne, D. J.; Ni, Z.; O'Keeffe, M.; Yaghi, O. M. *Angew. Chem., Int. Ed.* **2008**, *47*, 5136–5147. (c) Tyurin, V. S.; Yu, A.; Guilard, T. R.; Stern, C. *Chem. Rev.* **2009**, *109*, 1659–1713. (d) Wiest, O.; Harrison, C. B.; Saettle, N. J.; Cibulka, R.; Sax, M.; König, B. *J. Org. Chem.* **2004**, *69*, 8183–8185. (e) O'Neil, L. L.; Wiest, O. *J. Am. Chem. Soc.* **2005**, *127*, 16800–16801. (f) Gruber, B.; Stadlbauer, S.; Woinaroschy, K.; König, B. *Org. Biomol. Chem.* **2010**, *8*, 3704–3714.

(14) Burla, M. C.; Caliandro, R.; Camalli, M.; Carrozzini, B.; Cascarano, G. L.; De Caro, L.; Giacovazzo, C.; Polidori, G.; Spagna, R. *J. Appl. Crystallogr.* **2005**, *38*, 381–388.

(15) Sheldrick, G. M. *SHELX-97, Program for the Refinement of Crystal Structures*; University of Göttingen: Göttingen, Germany, 1997.

(16) Although the results of elemental analysis of **3** indicated that **3** includes 8 NO_3^-, 4 I^-, and 31 H_2O, only 4.932 NO_3^- and 8.540 H_2O were located in the crystal structure analysis (Table S6 in the Supporting Information).

(17) Martell, A. E.; Motekaitis, R. J. *The Determination and Use of Stability Constants*, 2nd ed.; Wiley-VCH: New York, 1992.

(18) Sun, L.; Martin, D. C.; Kantrowitz, E. R. *Biochemistry* **1999**, *38*, 2842–2848.

(19) (a) Zahn, S.; Reckien, W.; Kirchner, B.; Staats, H.; Matthley, J.; Lutzen, A. *Chem.—Eur. J.* **2009**, *15*, 2572–2580. (b) Tian, L.-L.; Wang, C.; Dawn, S.; Smith, M. D.; Krause, J. A.; Shimizu, L. S. *J. Am. Chem. Soc.* **2009**, *131*, 17620–17629.

(20) (a) Kitajima, N.; Moro-oka, Y. *Chem. Rev.* **1994**, *94*, 737–757. (b) Itoh, S. In *Comprehensive Coordination Chemistry II*; Que, L., Jr., Tolman, W. B., Eds.; Elsevier: Amsterdam, The Netherlands, 2003; Vol. 8; pp 369−393.

(21) We could not determine the pK_a values of Cu-bound water in **3** because of the very small change in the UV/vis spectra of **3** at pH 7−10 (Figure S7b in the Supporting Information).

(22) We have tested the self-assembly of **1** and copper using barbital, which has no hydrogen-bonding site, instead of CA. Very interestingly, it was found that Zn_2L, barbital, and Cu^{2+} automatically assemble to form a 2:2:2 complex, which has one μ-$Cu_2(OH)_2$ site, as confirmed by X-ray crystal structure analysis. Moreover, this 2:2:2 complex also accelerates the hydrolysis of MNP but was not catalytic. These results will be separately reported elsewhere.

(23) Stockbridge, R. B.; Wolfenden, R. *J. Am. Chem. Soc.* **2009**, *131*, 18248–18249.

(24) (a) Segel, I. H. *Biochemical Calculations*, 2nd ed.; John Wiley & Sons: New York, 1976. (b) Wong, C.-H.; Whitesides, G. M. *Enzymes in Synthetic Organic Chemistry*; Pergamon: Oxford, U.K., 1994. (c) Saier, M. H., Jr. *Enzymes in Metabolic Pathways: A Comparative Study of Mechamism, Structure, Evolution, and Control*; Harper & Row Publishers: New York, 1987. (d) Becker, W. M.; Kleinsmith, L. J.; Hardin, Bertoni, G. P. J. *The World of the Cell*, 7th ed.; Benjamin Cummings: San Francisco, 2008.

(25) As shown in Figure S10 in the Supporting Information, the thermodynamically determined K_d value of **3** with phenyl phosphate (~0.7 mM) is greater than the kinetic K_m value of MNP (ca. 470 μM). We assume that the reasons for the discrepancy between these two values would be because these parameters were determined in different methods and/or because the 4-nitrophenyl group of MNP may have some interactions (e.g., hydrophobic and/or $\pi-\pi$-stacking interaction) with the catalyst **3**.

(26) It is established that the coordination of BNP to a metal such as Zn^{2+} is much weaker than that of MNP to Zn^{2+}, possibly because of the lower basicity of the BNP monoanion than that of MNP (ref 27 and references cited therein).

(27) Kimura, E.; Aoki, S.; Koike, T.; Shiro, M. *J. Am. Chem. Soc.* **1997**, *119*, 3068–3076.

(28) Although we have tried electrospray ionization mass spectrometry (ESI-MS) measurement of the complex of **3** itself and the **3**-HPO_4^{2-} complex, the molecular-ion peaks corresponding to these species were not observed and only the molecular-ion peak corresponding to ($\mathbf{2}$-(NO_3^-))$^{3+}$ ([$(Zn_2L)_2(CA)_2NO_3$]$^{3+}$) was obtained from the ESI-MS spectrum of an aqueous solution of **3** (Figure S13 in the Supporting Information).